RESEARCH ARTICLE

ESPL **WILEY**

Streamlined subglacial bedform sensitivity to bed characteristics across the deglaciated Northern Hemisphere

Marion A. McKenzie[1] (ID) | **Lauren M. Simkins**[1] | **Sarah M. Principato**[2] |
Santiago Munevar Garcia[1]

[1]Department of Environmental Sciences, University of Virginia, Charlottesville, Virginia, USA

[2]Environmental Studies Department, Gettysburg College, Gettysburg, Pennsylvania, USA

Correspondence
Marion A. McKenzie, University of Virginia, Department of Environmental Sciences, Charlottesville, VA 22904-4123, USA.
Email: mm8dt@virginia.edu

Abstract

Streamlined subglacial bedforms observed in deglaciated landscapes provide the opportunity to assess the sensitivity of glacier dynamics to bed characteristics across broader spatiotemporal scales than is possible for contemporary glacial systems. While many studies of streamlined subglacial bedforms rely on manual mapping and qualitative (i.e., visual) assessment, we semi-automatically identify 11,628 sedimentary and bedrock bedforms, created during and following the Last Glacial Maximum across nine geologically and topographically diverse deglaciated sites in the Northern Hemisphere. Using this large dataset of landforms and associated morphometrics, we empirically test the importance of subglacial terrain on bedform morphology and ice-flow behavior. A minimum bedform length–width ratio threshold provides a constraint on minimum morphometrics needed for streamlined bedforms to develop. Similarities in bedform metric distribution regardless of bed properties indicate that all bed types may support similar distributions of warm-based ice flow conditions. Ice flow within valleys with easily erodible beds host the most elongate bedforms yet the widest range in bedform elongation and bedform surface relief. The presence of these highly elongate bedforms suggest high ice-flow velocities occur within valley settings despite spatially heterogeneous landform-generating processes. In contrast, lithified sedimentary beds within regions not constrained by topography on the scale of 1–10^2 km contain bedforms with high density and packing, low change in surface relief and low elongation, indicating spatially uniform and organized interactions at the ice–bed interface and consistency in ice-flow velocity. Regardless of genesis, we find a sensitivity of bedform elongation (i.e., used to interpret ice-flow speed or persistence) to topographic conditions on the scale of 1–10^2 km, while bedform density is sensitive to bed lithology. The findings presented in this study provide analogues for processes of subglacial erosion and deposition, ice–bed interactions and warm-based ice flow within contemporary glacial systems.

KEYWORDS
geomorphology, glacial landforms, ice flow, ice sheet, lithology, topography

1 | INTRODUCTION

Understanding the conditions that control ice-sheet flow is particularly important for ice streams, conduits of fast-flowing ice at rates of 10^2–10^3 m a^{-1}, due to their ability to efficiently drain and destabilize glacial catchments and greatly impact glacial contributions to sea level (Bamber & Aspinall, 2013; Rignot et al., 2019; Serrousi et al., 2017). The character of the underlying terrain (i.e., bed) beneath ice streams

influences ice-flow velocity and organization by modulating driving stresses, subglacial hydrology (Falcini et al., 2018; Greenwood et al., 2021; Hall & Glasser, 2003; Hindmarsh, 2001; Maier et al., 2019; Wellner et al., 2001) and spatial variations in ice thickness (Eyles et al., 2018; Payne & Dongelmans, 1997; Roberts et al., 2010). Patterns and rates of ice flow are commonly linked to known or perceived properties of the bed including topography and lithology (Clarke et al., 1977; Cuffey & Paterson, 2010; Whillians & van der Veen, 1997). Bed properties can have opposing effects and varying degrees of influence on ice-stream behavior (De Rydt et al., 2013; Falcini et al., 2018; Greenwood et al., 2021).

Valleys and troughs underlying both marine and terrestrial-based glacial systems have the potential to increase ice-flow velocities due to steering and thickening of ice, leading to increased pressure melting and overall meltwater abundance that enhance basal sliding and sediment deformation (Eyles et al., 2018; Hindmarsh, 2001). Similarly, ice flow is accelerated through strain heating of basal ice (McIntyre, 1985; Pohjola & Hedfors, 2003; Winsborrow et al., 2010) in areas of positive topographic relief (i.e., pinning points, ridges and banks) and regions of high bed roughness (i.e., spatial variation in surface elevation and slope; Falcini et al., 2018; Rippin et al., 2011; Siegert et al., 2005). In other circumstances, obstacles in the bed and deep valley regions surrounded by areas of high topographic relief enhance basal and lateral drag, leading to slower ice flow and potential grounding-line stabilization in marine-terminating systems (Falcini et al., 2018; Favier et al., 2016; Whillans & van der Veen, 1997).

Bed lithology also plays a fundamental role in ice–bed coupling, efficiency of meltwater transmission, and sedimentary processes such as deformation, erosion and deposition (Weertman, 1957). Permeable unlithified sedimentary beds allow for water infiltration and enhanced ice motion due to sediment deformation (Alley et al., 1986; Cuffey & Paterson, 2010; Tulaczyk et al., 2000), whereas more impermeable, "hard" beds facilitate sliding through liquid water being held between the ice and bed (Evans et al., 2006; Nienow et al., 2017). Rates of erosion and deposition in the subglacial environment are fundamentally impacted by bed lithology due to its control on meltwater transmission and, presumably, relative erodibility differences between different lithologies (Fowler, 2010; Greenwood & Clark, 2010; Ng, 1998).

Erosion and deposition at the ice–bed interface commonly creates subglacial streamlined bedforms, elongate in the direction of ice flow, which indicate sedimentary processes under variable glaciological conditions across landscapes (e.g., Alden, 1905; Charlesworth, 1957; Clark, 1993; Clark et al., 2009; Hollingworth, 1931; King et al., 2009; Menzies, 1979; Shaw et al., 1989; Spagnolo et al., 2010, 2011; Stokes & Clark, 2001, 2002; Wright, 1912). Genetic controls on streamlined bedforms include bed erosion by meltwater (Shaw et al., 2008), ice-keel ploughing (Clark et al., 2003; Tulaczyk et al., 2000), heterogeneous sediment deposition due to orthogonal basal pressure variability (Schoof & Clark, 2008), and till deformation (King et al., 2009). Because many bedform types, such as glacial lineations, are genetically and morphologically similar between contemporary and paleo-glacial systems (King et al., 2009), the location of former warm-based ice flow is interpreted from streamlined bedforms (e.g., Bourgeois et al., 2000; Briner, 2007; Clark, 1993; Clark et al., 2003; Ottesen et al., 2008; Principato et al., 2016; Spagnolo et al., 2014; Stokes et al., 2013; Stokes & Clark, 2001). Streamlined bedforms are commonly well preserved and

mark the final or most prominent phase of ice flow across the landscape (Clark, 1999; Winsborrow et al., 2010). Ranging in size from centimeters to several kilometers in length and from centimeters to tens of meters in amplitude, the elongation (i.e., ratio of length to width) of streamlined bedforms is commonly used to infer characteristics of ice-flow speed in deglaciated landscapes, while long-axis orientation is used to infer ice flow direction (e.g., Stokes & Clark, 2001, 2002; Zoet et al., 2021).

Streamlined bedforms in deglaciated landscapes are used to interpret ice-flow behavior (e.g., Clark et al., 2009, 2018; Dowling et al., 2015; Ely et al., 2016; Greenwood & Clark, 2010; Hättestrand et al., 2004; Spagnolo et al., 2012, 2014; Stokes et al., 2013) and used to understand ice–bed interactions applicable to contemporary glacial systems (e.g., Eyles et al., 2018; Greenwood et al., 2021). Qualitative (i.e., visually descriptive) and quantitative (i.e., morphometric and statistical) analyses of streamlined bedforms are arduous tasks as these bedforms have low, even sub-meter vertical relief and typically occur in "swarms" of tens to thousands of bedforms (Clark et al., 2018; Ely et al., 2016; Hughes et al., 2010). While automated mapping methods more quickly detect streamlined bedforms than traditional manual mapping techniques, only a subset of these methods have been systematically applied across multiple sites (e.g., Cazenave et al., 2008; Clark et al., 2009; Saha et al., 2011; Spagnolo et al., 2017; Wang et al., 2017). Our study uses topographic positioning index (TPI; Tagil & Jenness, 2008; Weiss, 2001) to calculate "neighborhood" elevation and slope variations to semi-automatically identify subglacial streamlined bedforms from nine deglaciated landscapes in the Northern Hemisphere (Figure 1). This large, geographically diverse dataset of streamlined bedforms contains both bedrock and sedimentary bedforms, encompassing a range of erosional and depositional processes associated with ice flow of four former ice sheets. We aim to identify the sensitivity of warm-based ice-flow conditions and subglacial processes to variable bed conditions. Substrate influence on warm-based ice flow is inferred from bedform relationships with bed topography and lithology, independent of bedform genesis concepts.

2 | METHODOLOGY

We examined nine study sites including (A) the Puget Lowland in Washington, USA, formerly glaciated by the southern Cordilleran Ice Sheet (CIS); (B) Northwestern Pennsylvania, USA and (C) Chautauqua, New York, USA, glaciated by the southern Laurentide Ice Sheet (LIS); (D) M'Clintock Channel, Canada; (E) Prince of Wales Island, Canada; (F) Nunavut, Canada, glaciated by interior reaches of ice streams, terminating at the margin of the LIS (Margold et al., 2018); (G) Bárðardalur, Iceland, glaciated by the Icelandic Ice Sheet; and (H) northern Norway and (I) northern Sweden, glaciated by the Fennoscandian Ice Sheet (Figure 1; Table 1). While all sites were glaciated during the Last Glacial Maximum (LGM; 23,000–19,000 years ago; Hughes et al., 2013) and the surface-exposed streamlined bedforms represent LGM and post-LGM ice flow, some bedforms may have formed during earlier glaciations or be multi-generational in nature. Because this process-based study focuses on resultant bedform morphology and distribution, we refrain from integrating absolute ages outlining when the bedforms formed or when the sites were deglaciated—information that does not exist for each study site and is therefore beyond the scope of this project.
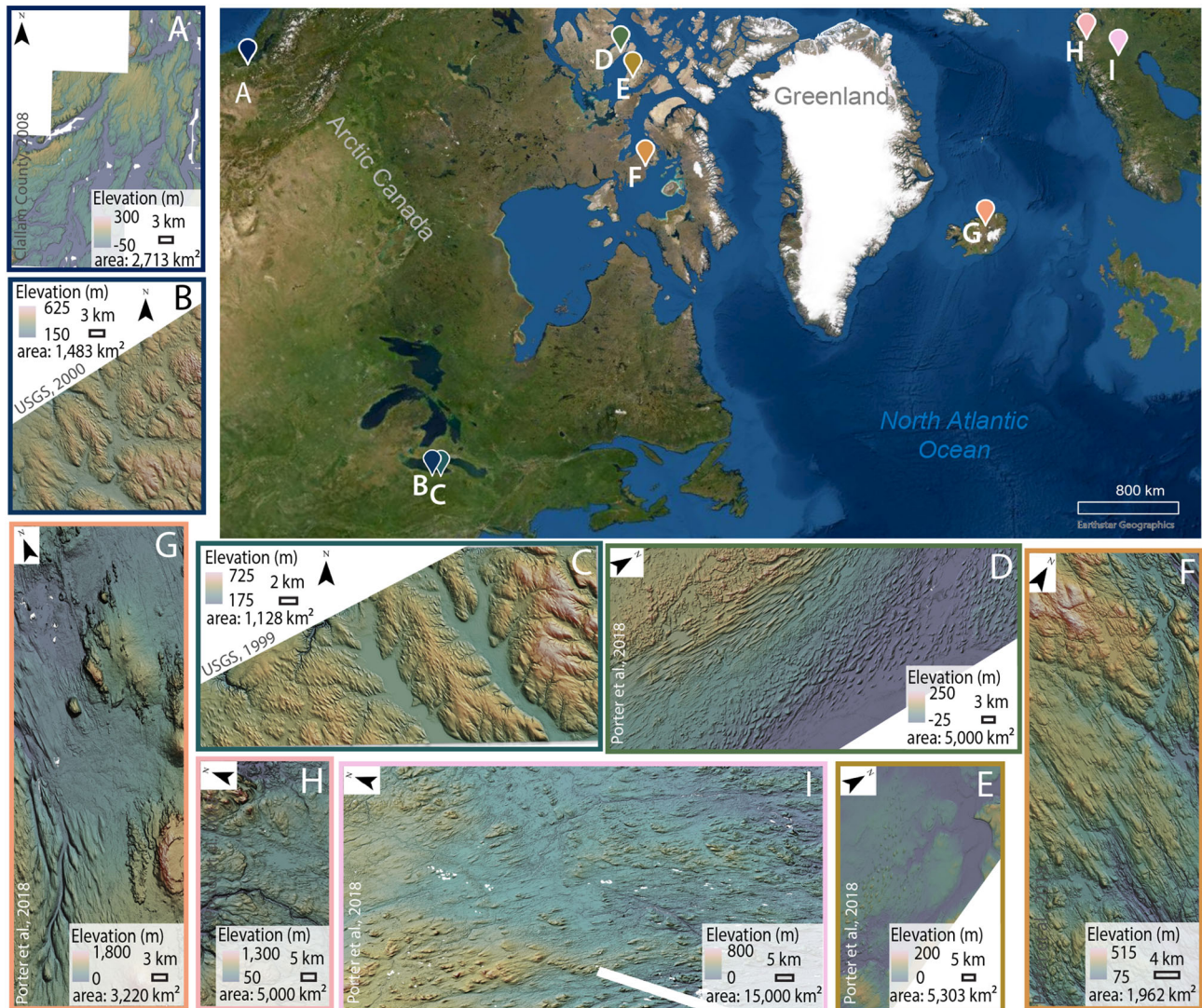
FIGURE 1 Study sites: (A) Puget Lowland, Washington, USA; (B) northwestern Pennsylvania, USA; (C) Chautauqua, NY, USA; (D) M'Clintock Channel, Canada; (E) Prince of Wales Island, Canada; (F) Nunavut, Canada; (G) Bárðardalur, Iceland; (H) northern Norway; (I) northern Sweden

Extensive efforts by state and national agencies to collect high-resolution digital elevation data allow for glacial landforms to be mapped at unprecedented spatial scales. Bed topography at each site was classified using publicly available digital elevation models (DEMs) with the highest clarity of 2 m vertical and 1.83 m × 1.83 m horizontal resolution and lowest clarity of 10 m vertical and 30 m × 30 m horizontal resolution, coupled with regional geology maps (Clallam County, Olympic Department of Natural Resources, WA, 2008; Porter et al., 2018; USGS, 1999, 2000). Present-day elevations of the DEMs differ from elevations at the time of glaciation due to glacial isostatic adjustment (GIA), tectonics and post-glacial landscape evolution; however, while absolute elevation differs from the LGM, relative relief at the streamlined bedform scale has not significantly changed. Visual hillshades for each DEM were created by utilizing ambient occlusion techniques, where multiple-scale and multi-directional hillshades were combined to create an incident lighting effect. This approach highlights the first-order detail on surface structures at different scales required to identify the wide range of streamlined bedforms presented here.

We classified topographic setting in the broadest sense as either "constrained" or "unconstrained" on spatial scales of 10^1–10^2 km

(Payne & Dongelmans, 1997). "Constrained" topography is defined as low elevation surrounded by more elevated regions on the horizontal scale of 1–10^2 km and vertical changes of at least 400 m from valley bottom to top, while "unconstrained" topography is defined as open, relatively uniform topography on the horizontal scale of 1–10^2 km with no more than 400 m of vertical elevation change across the site (Supporting Information Figure S1). Therefore, valleys, troughs and basins are considered constrained topography, while unconstrained topography lacks these features in the regional landscape.

Surficial bed lithology was generally classified as: "lithified sedimentary" including both clastic and carbonate bedrock; "crystalline"; "volcanic rock"; or, in one case, "mixed" bed including both crystalline and unlithified sedimentary beds. These distinctions were made due to the general variation in primary permeability, erodibility and likelihood of these lithologies to develop into a deformable subglacial bed. Unlithified sedimentary beds are the most permeable, erodible and likely to support a deformable bed, whereas the crystalline bedrock sites are the least permeable, erodible and least likely to contribute to the formation of a deformed till layer compared to a sedimentary bed. Only underlying bed composition was considered in determining site lithology; therefore, thin layers of till or soils overlying crystalline bed

TABLE 1 Site descriptions and data information

Site	Latitude, longitude	Bed setting	Topographic setting	LGM ice sheet	Land surface area (km^2)	Vertical resolution (m)	Horizontal resolution (m × m)
(A) Puget Lowland, Washington State[1]	122.8041731° W, 47.3591840° N	Mixed	Constrained	Cordilleran Ice Sheet	2,713	2	1.83 × 1.83
(B) Northwestern Pennsylvania[2]	79.9094684° W, 41.9908560° N	Lithified sedimentary bed	Unconstrained	Laurentide Ice Sheet	1,483	10	30 × 30
(C) Chautauqua, New York[3]	79.4920982° W, 42.1933209° N	Lithified sedimentary bed	Unconstrained	Laurentide Ice Sheet	1,128	10	30 × 30
(D) M'Clintock Channel, Canada[4]	106.0527872° W, 72.6426653° N	Lithified sedimentary bed	Unconstrained	Laurentide Ice Sheet	5,000	2	2 × 2
(E) Prince of Wales Island, Canada[4]	98.7397049° W, 72.2545398° N	Lithified sedimentary bed	Unconstrained	Laurentide Ice Sheet	5,303	2	2 × 2
(F) Nunavut, Canada[4]	83.5785928° W, 69.3271212° N	Crystalline bed	Unconstrained	Laurentide Ice Sheet	1,962	2	2 × 2
(G) Bárðardalur, Iceland[4]	17.4280416° W, 65.1232720° N	Volcanic bed	Constrained	Icelandic Ice Sheet	3,220	2	2 × 2
(H) Northern Norway[4]	23.6397066° E, 69.6518249° N	Crystalline bed	Constrained	Fennoscandian Ice Sheet	5,000	2	2 × 2
(I) Northern Sweden[4]	22.4763304° E, 67.0992965° N	Crystalline bed	Unconstrained	Fennoscandian Ice Sheet	15,000	2	2 × 2

Data sources: [1]Clallam County, Olympic Department of Natural Resources, WA, 2008; [2]USGS, 2000; [3]USGS, 1999; [4]Porter et al., 2018.

sites were not considered in bed lithology classification. While there are differences in properties between, for example, clastic and carbonate sedimentary rocks, the differences are subtle enough for the two categories to be classified together for the purpose of this regional and bedform-assemblage scaled work.

We mapped streamlined bedforms from the nine sites with a combination of manual identification and a novel semi-automated application of a TPI mapping tool, originally developed for the purpose of characterizing watersheds across regional landscapes (Weiss, 2001). TPI utilizes DEM cell elevation and mean elevation of a defined neighborhood to calculate slope variations across a landscape. Annulus neighborhood sizes were determined by assessing the visible range in scales of bedforms present. At least two neighborhood assessments, ranging from 300 to 2100 m, were conducted for each site and determined separately for each site based on the overall elevation range of the landscape and visual estimates of streamlined bedform metrics. Once the inner and outer neighborhood radius is defined, TPI calculates the mean elevation across the defined neighborhood for each pixel. A standardization is then used across the entire map to ensure varying sites are comparable. The tool, built using ArcPython code and ArcGIS ModelBuilder, was published for use (McKenzie et al., 2022). After standardization, TPI values above zero represent areas higher than surrounding topography, while negative TPI values measure locations lower than their surroundings. Using spatial analyst tools, all positive relief features identified by TPI, including features other than non-subglacial streamlined bedforms,

were separated into a polygon file (McKenzie et al., 2022; Supporting Information Figure S2). Thresholding of TPI-mapped bedform metrics such as feature length, width, orientation and area attributes coupled with a manual assessment, conducted by visually removing incorrectly identified features and adding features missed by TPI, resulted in a more accurate dataset whose metrics were not influenced by morphometric threshold sorting (McKenzie et al., 2022; Figure S2).

For each mapped bedform, its long-axis length and orientation, width orthogonal to length, and the range in elevation along the landform's long axis (termed here "bedform surface relief") were calculated automatically in ArcGIS Pro using the "Minimum Bounding Geometry" and "Add Z Information" tools. Automatic calculation of streamlined bedform long-axis cardinal orientation is quantified in degrees, measured by the rotation of the bedform long axis from due north, and is used to infer direction of ice flow (Clark, 1997; Kleman et al., 2006; Kleman & Borgström, 1996). Parallel conformity, or the standard deviation of an entire streamlined bedform dataset's orientation values at a given site, was additionally calculated in Excel. Bedform elongation ratio, calculated by dividing the bedform length by its width, and parallel conformity (i.e., the standard deviation of bedform orientation) were calculated in Excel. Defining bedforms solely by their shape rather than composition is a strength to this study, as it allows for the assessment of topographic and lithologic controls on ice streaming and sedimentologic and geomorphologic processes regardless of landform-generating processes that have been inferred for individuals or groups of landforms.

Statistical analyses including a linear Pearson correlation and Shapiro–Wilk test were conducted in "R" to compare bedform metric distributions. Qualitative metrics, namely site topography and lithology, were assigned a fixed numerical value that was used in the Pearson correlation, where topographically unconstrained regions were assigned a value of 0 and topographically constrained were assigned a value of 1. Sedimentary bedrock was assigned a value of 0, crystalline bedrock a 1, volcanic bedrock a 2 and mixed lithology a 3.

3 | RESULTS

In the following subsections, we demonstrate our use of TPI to identify streamlined subglacial bedforms, the trends and correlations of bedform morphology across all sites, and the relationship between spatial orientation and distribution of bedforms. Lastly, we describe the relationship between bedform characteristics and bed topography and lithology.

3.1 | Streamlined subglacial bedform identification

Across the nine sites, TPI identified 7,635 bedforms, while 3,993 bedforms were manually mapped (i.e., added or adjusted from TPI mapping), resulting in a total dataset of 11,628 sedimentary and bedrock bedforms (Figure 2). Of the nine study sites, the Puget Lowland (Site A) and M'Clintock Channel (Site D) sites had the highest proportion of bedforms correctly mapped by TPI as determined by visual inspection, requiring a lower percentage of false-positive bedforms to be manually removed (Table 2; Supporting Information Figure S3). Sites with low variation in site elevation, such as those in northwestern Pennsylvania (Site B) and Chautauqua (Site C), required the least manual bedform mapping (Figure 2; Table 2). In northern Sweden (Site I), the number of bedforms considered incorrectly identified by TPI exceeded the number of those that were considered correctly identified. Sites with the greatest number of bedforms manually added to the final dataset include northern Norway (Site H) and northern Sweden (Site I). There was no statistical significance between the proportion of TPI-identified false positives and the proportion of bedforms manually added to bed topography and lithology across the sites. Almost all scales of known streamlined bedforms (Ely et al., 2016) are resolved by DEMs and potentially identified by TPI, except for bedforms with millimeter to centimeter surface relief. The lowest relief of bedform surface mapped by TPI is <1 m, providing confidence in the ability of these dual methods to capture a "full" dataset of streamlined subglacial bedforms (Supporting Information Figure S3).

3.2 | Bedform morphology

The streamlined bedforms range in length from 94 to 15,388 m (mean 1,052 m; median 754 m) and in width from 19 to 2,323 m (mean 219 m; median 157 m). As determined by a linear Pearson correlation, bedform length and width have a positive correlation coefficient (Figure 3). This statistical analysis was fitting for this data as it met the assumption that all groups were statistically significant in their difference from one another ($p < 0.05$). Puget Lowland (Site A) bedforms span the greatest range in width and length of all sites, while Chautauqua (Site C) has the smallest ranges of length and width. Interestingly, low bedform lengths and widths are common for all sites, while bedforms with lengths greater than ∼2000 m and widths greater than ∼600 m are less common (Figure 4A).

A minimum ratio of length to width (i.e., elongation; e.g., Clark et al., 2009; Ely et al., 2016) of 1.12:1 is distinct for all sites. Consistency in peak elongation ratios for all sites is also observed, with a median elongation ratio of 5:1 (Figure 5; Table 2). The degree of positive skewness of elongation varies by site, with sites Bárðardalur (Site G) and northern Sweden (Site I) highly skewed, while sites Chautauqua (Site C) and northwestern Pennsylvania (Site B) are the least positively skewed, as determined by a Shapiro–Wilk normality test. The northern Norway (Site H) site has the highest mean and median bedform elongation ratio values, while Bárðardalur (Site G) has the greatest range of elongation ratio of all sites (Figure 6B; Hoffmann, 2015). Chautauqua (Site C) bedforms have the smallest elongation ratio mean, median and range of all sites (Figure 6B, Hoffmann, 2015). Bedform length and elongation as well as bedform length and width are positively correlated (Figure 3).

The Puget Lowland (Site A) has the highest mean, median and range of individual bedform surface relief than any other site (Figure 6A; Hoffmann, 2015). Prince of Wales Island (Site E) has the smallest mean and median bedform surface relief, while M'Clintock Channel (Site D) has the smallest bedform surface relief of all sites (Figure 6A: Hoffmann, 2015). Bedform length and bedform surface relief have a strong positive correlation coefficient (Figure 3). When comparing individual bedform elongation and bedform surface relief, more elongate bedforms correspond to more uniform bedform surface relief (Figure 4C,D). Conversely, less elongate bedforms display greater variation in individual bedform surface relief (Figure 4D).

3.3 | Bedform parallel conformity and distribution

While streamlined bedform orientations vary by site depending on predominant direction of ice flow, the average parallel conformity (i.e., standard deviation of orientation) of all sites is 26° (Figure 7). Multiple sites, including M'Clintock Channel (Site D) and Prince of Wales Island (Site E), have notable variations and cross-cutting relationships between bedforms of different orientations, indicating two temporally distinct flow orientations, although one flow orientation is far more prominent (Figures 2 and 7). Two of the topographically constrained sites, Bárðardalur (Site G) and northern Norway (Site H), are clearly influenced by topographic steering of bedform orientation (Figure 7). Swarms of bedforms at M'Clintock Channel (Site D) are more elongate in the center of the mapped clusters than the edges, while bedform elongation at all other sites varies without apparent spatial organization. At M'Clintock Channel (Site D), where we see this spatial organization of bedform elongation, the bedforms also express high parallel conformity and high density and packing (Figure 8; Table 2).
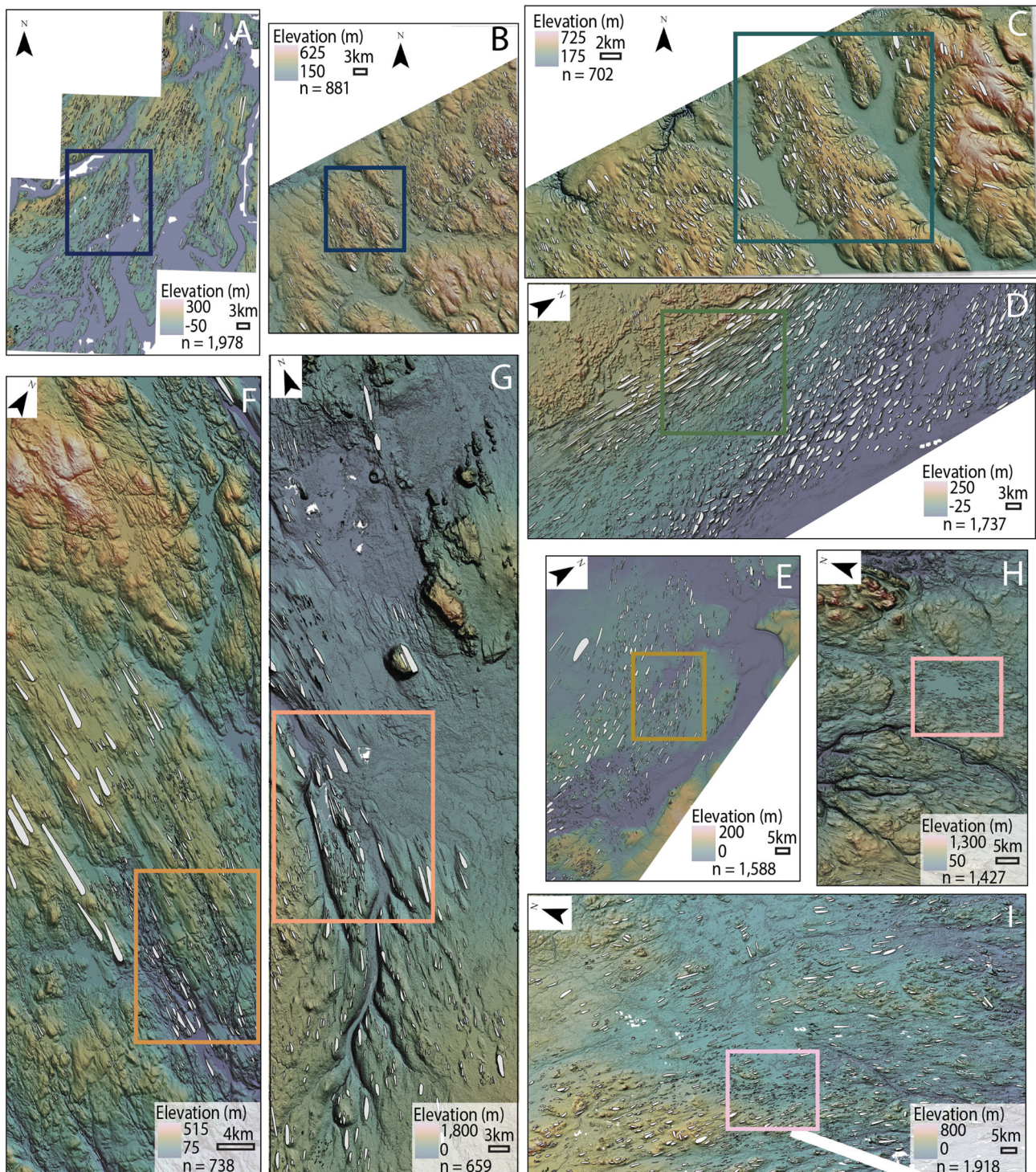
FIGURE 2 Streamlined subglacial bedforms (gray polygons) at sites (A) Puget Lowland, Washington, USA; (B) northwestern Pennsylvania, USA; (C) Chautauqua, NY, USA; (D) M'Clintock Channel, Canada; (E) Prince of Wales Island, Canada; (F) Nunavut, Canada; (G) Bárðardalur, Iceland; (H) northern Norway; (I) northern Sweden. Outlined inset boxes are locations shown in Figure 8

3.4 | Bedform morphometric correlations with bed lithology and topography

The Puget Lowland (Site A), a topographically constrained mixed lithology site, has the greatest number of bedforms per area (i.e., density) and the highest bedform area per area (i.e., packing; Table 2) compared to the eight other sites. Altogether, the topographically unconstrained sites with sedimentary bedrock have the next highest packing or density values (Table 2).

The topographically constrained volcanic bed of Bárðardalur (Site G) contains low-density and packing bedform swarms and has the most elongate bedforms in the dataset (Figure 8; Table 2). After Bárðardalur (Site G), the sites with the most elongate bedforms are also all topographically constrained sites (Table 2). Utilizing a linear Pearson correlation, constrained topography has a high positive correlation coefficient with elongation and bedform surface relief, while unconstrained topography is correlated with greater bedform width (Figure 3). Bed lithology has a strong negative correlation coefficient,

TABLE 2 Bedform data by site, including mapping statistics and bedform metrics

Site	Number of bedforms (nremoved; nadded)	Number of final bedforms per 10 km²	Bedform area (km²) per 10 km²	% bedforms mapped manually	% TPI mapped false positives	Mean length ± standard deviation	Mean width ± standard deviation	Mean elongation	Parallel conformity
(A) Puget lowland, Washington state — V, mixed bed lithology	1,978 (512; 401)	7.3	3.8	20	20	2,013 ± 1,261	365 ± 180	5.9	27
(B) Northwestern Pennsylvania — **O, sedimentary bedrock**	881 (774; 60)	5.9	0.5	7	50	666 ± 342	162 ± 69	4.4	11
(C) Chautauqua, New York — **O, sedimentary bedrock**	702 (493; 103)	6.2	0.7	10	50	652 ± 337	164 ± 77	4.1	10
(D) M'Clintock Channel, Canada — **O, sedimentary bedrock**	1,737 (333; 615)	3.5	1.1	40	20	1,259 ± 789	278 ± 153	5.0	31
(E) Prince of Wales Island, Canada — **O, sedimentary bedrock**	1,588 (1,657; 665)	3.0	0.8	40	60	1,054 ± 882	224 ± 162	4.9	51
(F) Nunavut, Canada — **O, crystalline bedrock**	738 (>800; 155)	3.8	0.3	20	60	617 ± 614	115 ± 88	5.4	7
(G) Bárdardalur, Iceland — **V, volcanic bedrock**	659 (745; 326)	2.1	0.3	50	50	1,006 ± 701	175 ± 125	6.6	59
(H) Northern Norway — **V, crystalline bedrock**	1,427 (526; 783)	2.9	0.3	50	50	842 ± 580	132 ± 68	6.9	17
(I) Northern Sweden — **O, crystalline bedrock**	1,918 (2,241; 858)	1.3	0.6	50	70	1,324 ± 794	346 ± 187	4.1	19

Across site bed settings, a "**V**" denotes a topographically constrained site, while "**O**" denotes a topographically unconstrained site. Parallel conformity is a measurement of the standard deviation of mean orientation.

with bedform width indicating that large widths are likely on sedimentary bedrock sites while bedforms with smaller widths are more common in mixed lithology sites. Conversely, bedform surface relief is highly correlated with surface lithology, where sedimentary bedrock sites have lower bedform surface relief and mixed lithology sites have greater bedform surface relief (Figure 3). Regardless of these differences, all sites have similar morphometric distributions and show considerable overlap with common means and medians, rather than distinct populations, and only differ in the degree of skewness.
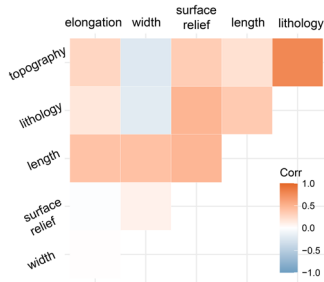

FIGURE 3 Correlation matrix of all 11,628 bedform features, conducted using linear Pearson correlation. Categorical variables were assigned arbitrary values for comparison statistics

4 | DISCUSSION

A discussion of the performance of TPI in mapping subglacial streamlined bedforms is presented in the first subsection, followed by discussions of streamlined bedform morphology and the relationship between bedform morphology and bed settings.

### 4.1 | Success of semi-automatic mapping streamlined bedforms in deglaciated landscapes

Previous morphometric studies of streamlined subglacial bedforms have utilized Fourier spectra data (e.g., Spagnolo et al., 2017), manual identification (e.g., Principato et al., 2016), object-oriented automatic identification (e.g., Saha et al., 2011), contour-tree mapping (Wang et al., 2017) and other methods systematically utilized to identify bedforms across singular and multiple geographic locations (e.g., Clark et al., 2009, 2018; Ely et al., 2016; Greenwood & Clark, 2010; Spagnolo et al., 2014; Stokes et al., 2013). While TPI was originally developed to classify landscapes and delineate watersheds (Tagil & Jenness, 2008; Weiss, 2001), its ability to characterize negative and positive relief features through slope variations is conceptually
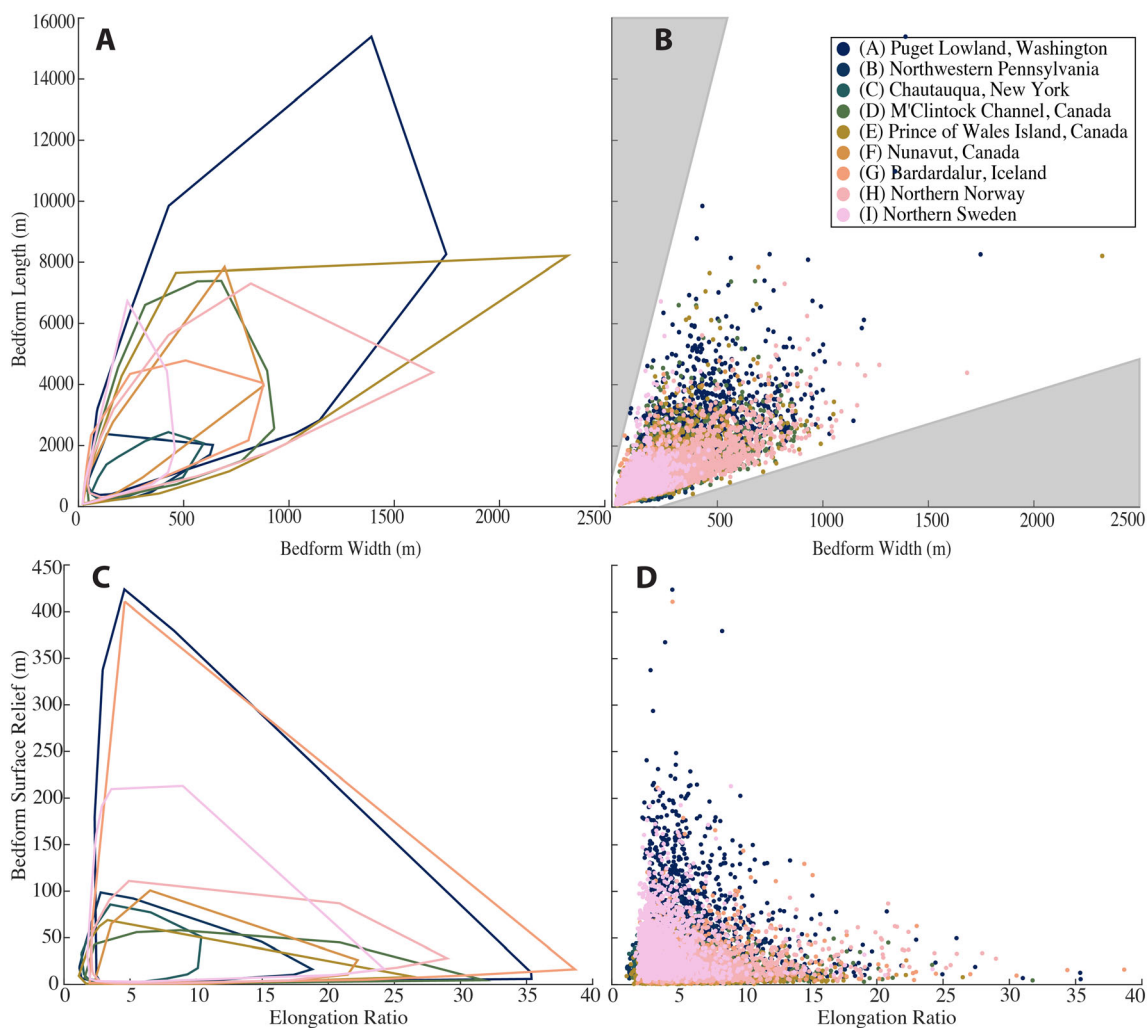
FIGURE 4 Bedform length and width metrics plotted by site: (A) convex hull area of all bedform length and width metrics and (B) scatterplot of the same data as (A); gray areas indicate regions where bedforms are not observed. (C) Convex hull area of all bedform elongation ratio and elevation range metrics; (D) scatterplot of the same data as (C)
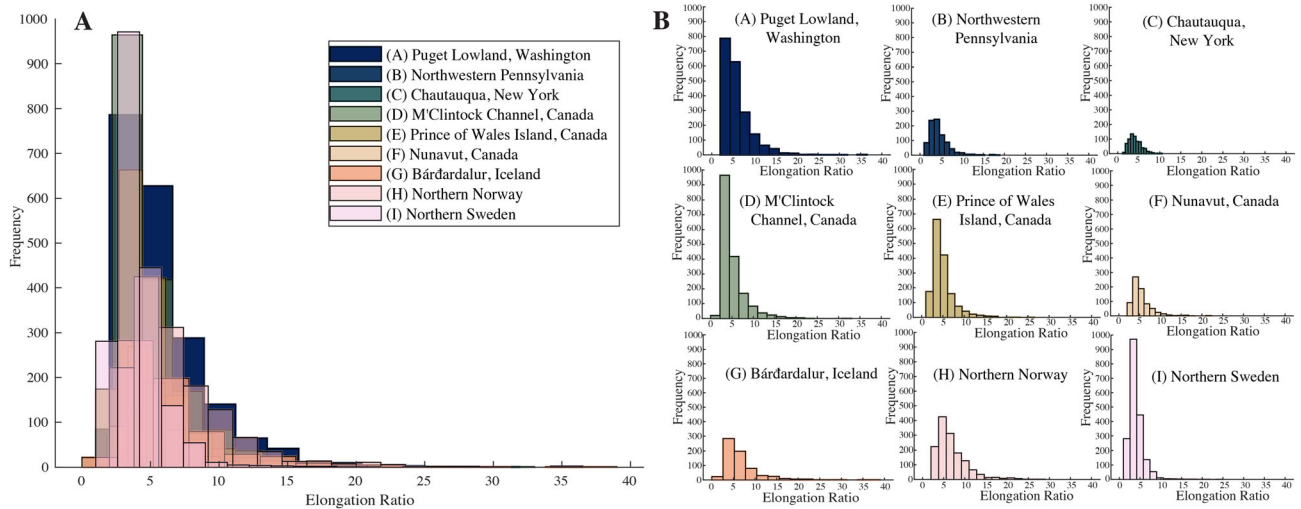
FIGURE 5 Frequency (*n*) of bedform elongation ratios. (A) Composite histograms of elongation frequencies for each site. (B) Individual site elongation frequencies. Site bins were determined by the "nbins" function in MATLAB, assigning each site 15 bins in order to make frequencies comparable
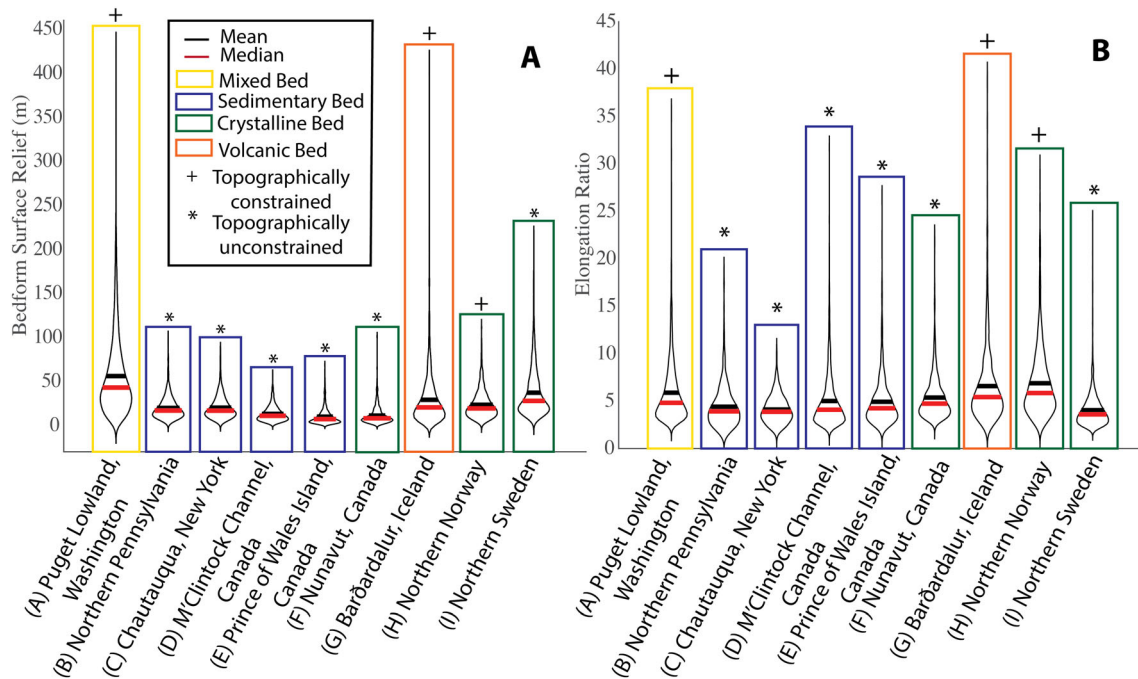

FIGURE 6 (A) Distribution of bedform surface relief range and (B) distribution of bedform elongation ratios by site characterized by topography and bed substrate. MATLAB code for violin plot visualization sourced from Hoffmann (2015)

applicable to many landscapes. In the context of glacial landscapes, the distinct elongate morphologies and occurrence of numerous bedforms in close proximity make streamlined subglacial bedforms well suited for identification with TPI. In general, highly elongate bedforms with low bedform surface relief are more difficult to map due to small and narrow slope differentiations. Due to the difficulty of the TPI method in identifying these sizes of bedforms, many of the manually mapped bedforms were visually low-relief and highly elongate (Figure S3). Additionally, two sites with the greatest number of manually mapped bedforms occurred in northern Norway (Site H) and northern Sweden (Site I; Table 2), where preservation of non-glacial or minimally glacially

modified landforms is significant across the entire region (Ebert et al., 2012; Hall et al., 2013; Kleman & Stroeven, 1997). These mapping challenges may be a result of residual pre-LGM landform assemblages and bedrock morphologies from pre-Quaternary formation and weathering processes (e.g., Ebert et al., 2012; Hall et al., 2013; Kleman & Stroeven, 1997). Landscape features that were manually removed include non-glacial positive relief features such as modern riverbanks and isolated bedrock highs, identified by their location, size, orientation or lack of any elongation. While there were some shortcomings in the bedform TPI identification method developed for this work, the hundreds of hours saved by semi-automatically identifying
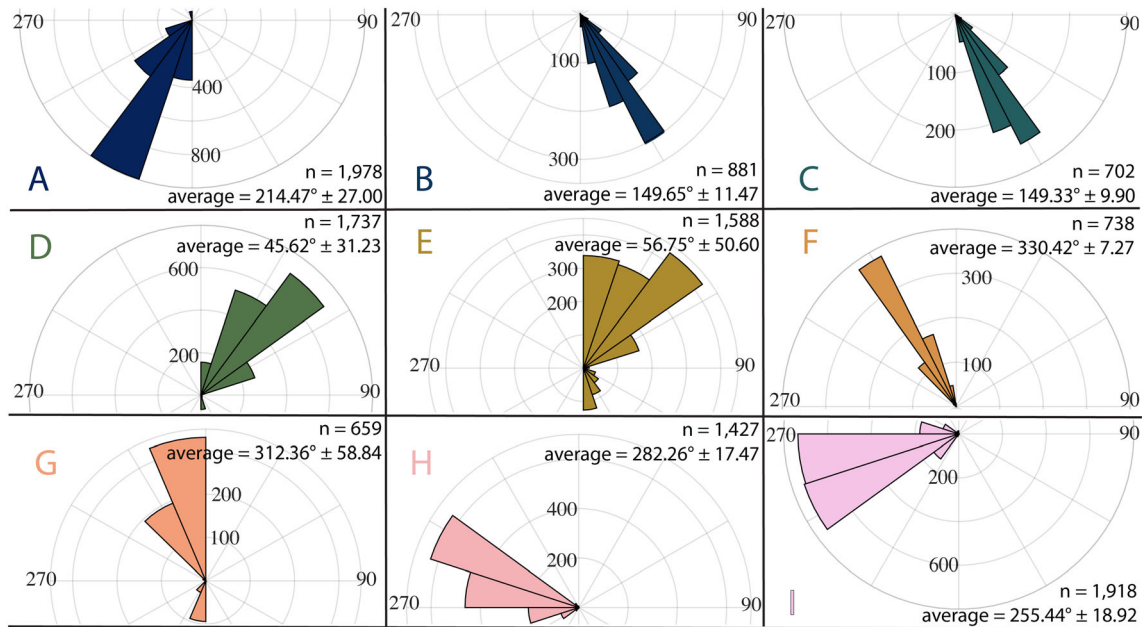
FIGURE 7 Cardinal orientations of mapped bedforms. (A) Puget Lowland, Washington, USA; (B) northwestern Pennsylvania, USA; (C) Chautauqua, NY, USA; (D) M'Clintock Channel, Canada; (E) Prince of Wales Island, Canada; (F) Nunavut, Canada; (G) Bárðardalur, Iceland; (H) northern Norway; (I) northern Sweden
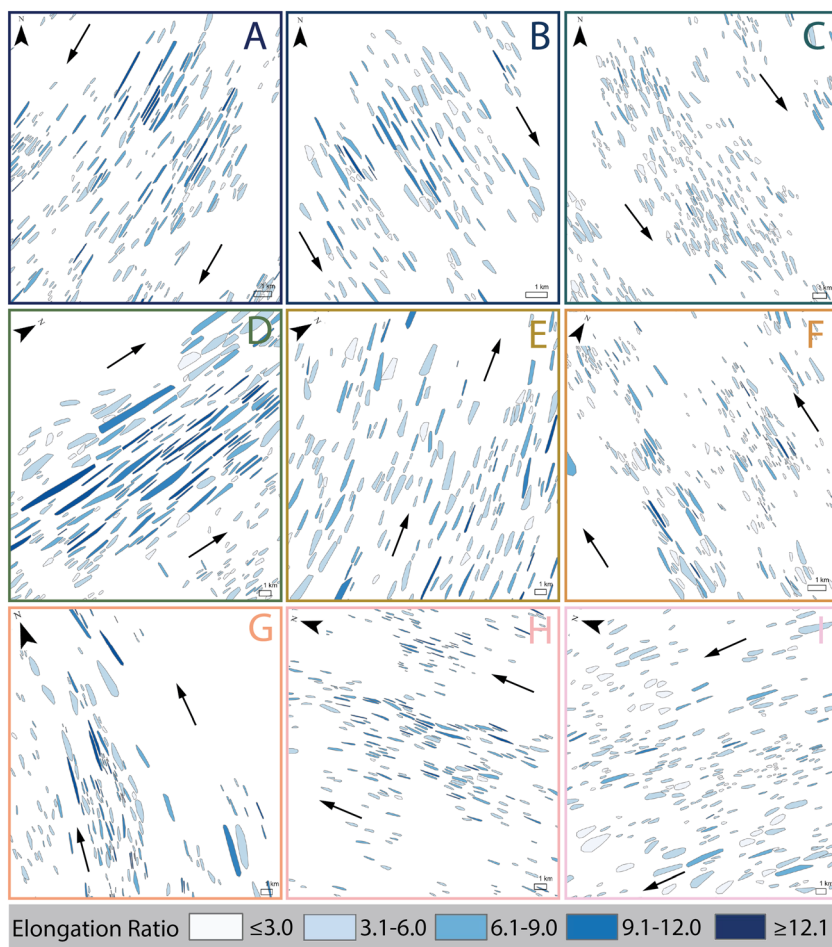
FIGURE 8 Representative bedform elongation ratios at (A) Puget Lowland, Washington, USA; (B) northwestern Pennsylvania, USA; (C) Chautauqua, NY, USA; (D) M'Clintock Channel, Canada; (E) Prince of Wales Island, Canada; (F) Nunavut, Canada; (G) Bárðardalur, Iceland; (H) northern Norway; (I) northern Sweden. Black arrows indicate ice flow direction

these bedforms renders this tool highly useful. Use of the TPI identification tool also reduces investigator bias through its systematic identification of positive relief features across a landscape.

While the percentage of bedforms incorrectly mapped by TPI has no correlation to site topography or lithology (Table 2), the crystalline bed sites in northern Norway (Site H) and northern Sweden (Site I) and

volcanic bedrock site in Bárðardalur (Site G) had the greatest proportion of their bedforms identified manually (Table 2). The hard beds in Sweden and Norway, less easily eroded, preserve a landscape legacy of older and persistent processes and therefore have many large, high relief features such as inselbergs (e.g., Ebert et al., 2012; Hall et al., 2013). High-relief features dominate the landscape, even in areas impacted by glacial processes. Therefore, glacial features left on the surface are often very subtle and low in relief, creating difficulties for TPI to identify these small relief bedforms amidst the more pronounced, high-relief features of these landscapes, making manual identification more suitable for these types of bedforms. TPI, therefore, does not perform as well on crystalline bedrock sites as it does on sedimentary bedrock sites where glacial erosion has a larger impact on surface relief. It is also important to note that the crystalline bedrock sites (Sites F, H, I) were deep in the ice sheet interior, where cold-based ice is thought to have been prevalent for long periods over multiple glaciations. Therefore, not only was the crystalline bedrock difficult to erode, but the glaciological environment did not support streamlined bedform processes (Margold et al., 2015; Stokes & Clark, 2001). For a similar reason, the large proportion of manually mapped bedforms in Bárðardalur (Site G) could, in part, be due to a variety of bedform composition and relief ranging from low-relief features comprised entirely of diamicton to high-relief features comprised of diamicton overlaying bedrock cores formed during rifting. More pronounced, high-relief features are more easily identified by TPI mapping, while low relief features are not as easily delineated by the tool.

4.2 | Bedform properties across the deglaciated Northern Hemisphere

While sub-meter relief bedforms like bedrock striations are not resolved in the dataset presented here, meter to kilometer-scale bedforms like drumlins and flutes are well resolved. Bedforms across the datasets have significant overlap and positive correlation between width and length (Figures 3 and 4A,B), indicating a shared genetic mechanism between bedforms regardless of their composition or whether they formed through erosional or depositional processes. Additionally, both length and width data are positively skewed, with more small bedforms than large (Figure 4A,B). This process of bedform elongation is commonly referenced in the field and has led to the use of elongation as a proxy for ice streaming velocity and length of time that a particular flow regime has been operating (e.g., Benediktsson et al., 2016; Livingstone et al., 2016; Stokes et al., 2013; Stokes & Clark, 2002).

Although our nine study sites were glaciated by different ice sheets on different continents, resulting subglacial bedforms were found to be morphologically similar (e.g., Stokes & Clark, 2002; Clark et al., 2009; Saha et al., 2011; Spagnolo et al., 2014; Principato et al., 2016). The similarities in quantitative bedform morphometrics across the study sites suggest similar genetic relationships between all streamlined subglacial bedforms. In this study, we find a minimum length to width ratio (i.e., elongation; e.g., Clark et al., 2009; Ely et al., 2016) of 1.12:1, indicating that barely elongate bedforms are (1) resolved in the dataset and (2) occur for the full size range of bedforms (Figure 4A,B) potentially due to the highly dynamic and rapidly evolving bedform development beneath warm-based ice (Stokes et al., 2013). In other terms, we observe that a large bedform can be

equally as stunted as a small one, suggesting that growth of bedforms does not necessarily add length or strip width preferentially and there is not one single style of bedform development. The unimodal distribution of elongation ratios with positive skewness seen in this work, indicating a continuum of bedform types, has also been found in other morphological bedform assessments (Figure 5; e.g., Clark et al., 2009; Saha et al., 2011; Stokes et al., 2013; Spagnolo et al., 2014; Ely et al., 2016; Principato et al., 2016).

We find that less elongate bedforms are interspersed with more elongate features and not present at the margins of bedform swarms (Figure 9). This result is not unique and has been hypothesized to be a result of the rapidly changing subglacial dynamics responsible for bedform formation and development (Rattas & Piotrowski, 2003; Stokes et al., 2013). An exception of this observation is at M'Clintock Channel (Site D), where the largest, most elongate bedforms at this site are spatially centered in the middle of the mapped bedform swarm, while the least elongate bedforms flank the lateral edges (Figure 8). This spatial organization likely represents a centralized zone of stronger ice streaming, where lateral drag slowed ice flow along the edges. At the M'Clintock Channel site (Site D), we see direct evidence for ice streaming where fast-flowing ice is bounded by slower moving ice (Margold et al., 2018). The spatial organization of elongation at M'Clintock Channel (Site D) contains classic assemblage characteristics associated with fast-flow corridors (e.g., Spagnolo et al., 2014; Stokes et al., 2013; Stokes & Clark, 2001, 2002, 2003).

While particularly notable at topographically constrained and easily eroded bed substrates, all sites showcase a trend of more elongate bedforms corresponding to lower bedform surface relief (Figure 4C, D). This pattern is an indication of ice-flow persistence (Benediktsson et al., 2016), whereby persistent erosion and deposition at the ice–bed interface in conjunction with warm-based ice flow produce a flat bedform feature. Conversely, less elongate bedforms correlate with greater variability in bedform relief (Figure 4C,D), suggesting areas of faster-flowing ice have a glaciological control of more persistent and uniform organization of subglacial erosion and deposition. Therefore, in areas where ice streaming is not persistent or stable or ice velocities are relatively slow, erosion and depositional processes are more spatially heterogeneous to result in uneven individual bedform surface relief. Controls on the occurrence of bedform development may be directly related to variations in bed lithology (Greenwood & Clark, 2010) and topography (Falcini et al., 2018; Favier et al., 2016; Whillans & van der Veen, 1997) or could be indirectly related through substrate control on glaciologic processes. However, this distinction was not explicitly assessed for individual bedforms within this study.

4.3 | Bedform morphology in relation to bed setting

Spatially stable and persistent ice streaming conceptually contributes to spatial homogeneity in erosion and deposition processes, leading to the formation of consistently orientated and shaped bedforms. Deviations to bedform orientation occur from both temporal and spatial variations, where bedforms can be preserved from multiple glaciations, such as in northern Sweden (Site I), or across constrained topography, such as in the Puget Lowland (Site A), Bárðardalur (Site G) and northern Norway (Site H). Regions with highly elongate bedforms correspond to

qualitatively greater flow orientation organization (Figures 6 and 8; Table 2), which is potentially attributed to multi-generational or persistent bedform formation and development. Multiple glaciations in the same orientation produce more uniformly oriented features (i.e., higher parallel conformity). In the case of spatially influenced orientation, topographic constrains on ice-flow develops bedform clusters with orientation that reflects the orientation of the valley in which it is constrained, such as in Bárðardalur (Site G).

Findings from previous work on bedform presence and morphologies identify glaciological drivers as fundamental controls on bedform morphology via subglacial processes, while others identify direct substrate control on resulting bedform morphologies due to inherent characteristics in the bed (e.g., Greenwood & Clark, 2010; King et al., 2009; Rattas & Piotrowski, 2003; Stokes et al., 2013). Qualitatively soft, more permeable and easily eroded beds allow for greater production and transport of sediment to the ice margin (Clark, 1993; Rattas & Piotrowski, 2003; King et al., 2009; Livingstone et al., 2016). The abundance of deformable till forming from the permeable environments of both lithified and unlithified sedimentary beds explains the presence of high-density bedforms in the regions with unlithified sediment (King et al., 2009; Stokes et al., 2013). Conversely, "hard," crystalline beds are generally more resistant to erosion (Eyles & Doughty, 2016; Krabbendam et al., 2016) and more likely to have "fixed" bedforms resistant to sediment production and transport (Zoet et al., 2021). The greatest number of bedforms per area, present on a mixed (unlithified sedimentary bed system with crystalline bedrock) bed in the Puget Lowland (Site A), likely occur due to high availability of unlithified sediments and meltwater presence from strain heating. Strain heating occurs as ice flows over bedrock highs, collectively allowing for greater bed erosion across the permeable unlithified sediment, material deposition and subsequent ice streaming (McIntyre, 1985; Pohjola & Hedfors, 2003; Winsborrow et al., 2010). In addition to the mixed bed site, lithified sedimentary beds were also densely populated with streamlined bedform features (Table 2). Crystalline and volcanic beds in both constrained and unconstrained topographic settings have the lowest bedform densities, suggesting that bed lithology, rather than topography, is a more dominant control on streamlined bedform density. However, it remains unclear and difficult to assess whether bed substrate controls either sedimentary processes regardless of flow regime or whether substrate controls streaming conditions. In either case, a distinct bedform signature across a particular bed substrate is produced.

The unimodal and positively skewed distribution of bedform elongation indicates that similar distributions of elongation occur at a multitude of sites regardless of bed topography and lithology or climatological and glaciological factors (Table 1; Figure 4A,B; e.g., Clark et al., 2009; Ely et al., 2016; Principato et al., 2016; Saha et al., 2011; Spagnolo et al., 2014; Stokes et al., 2013). The minimum elongation threshold and similarity in relative elongation distribution across sites highlight a similarity of ice–bed interactions across "soft" and "hard" beds in both topographically confined and unconfined settings, suggesting a self-organization of ice–bed processes regardless of site characteristics. The concept of streamlined bedforms developing as a self-organizing phenomenon is not novel in the field of glacial geomorphology and has been suggested to occur independently from local bed lithologic and topographic conditions (Clark, 2010; Spagnolo et al., 2017; Clark et al., 2018). This independent organization is well represented by the unit-less elongation ratio and allows for comparison of warm-based ice-flow velocities or persistence between individual sites. Differences in elongation distributions across sites of variable topography or bed lithology would suggest an influence of substrate on bedform formation and development or substrate influence of glaciologic processes at the bed. However, from the similarities in bedform elongation distribution we see here and in previous work, we suggest that regions of warm-based ice flow, leading to the development of streamlined subglacial bedforms, exhibit potential for equivalent relative ice-flow velocity distribution or persistence of ice-flow pathways regardless of bed character.

While all sites have similar elongation distribution trends, topographically constrained sites produce bedforms with the highest mean and median elongation ratios with the most elongate bedforms of the overall dataset (Figure 6B; Tables 1 and 2). Topographic constraint on ice flow results in topographic funneling and increased ice speed (Hindmarsh, 2001; Wellner et al., 2001; Hall & Glasser, 2003; Ottesen et al., 2008; Roberts et al., 2010; Eyles et al., 2018). While bedform elongation is enhanced in regions that are topographically constrained, bedform elongation is not contingent on bedrock substrate (Figure 6B; Tables 1 and 2), which we interpret to reflect a higher sensitivity of warm-based ice-flow velocity and persistence to bed topography than bed substrate (Greenwood et al., 2021; Halberstadt et al., 2016; Ignéczi et al., 2018; Serrousi et al., 2017; Stokes & Clark, 2003; Winsborrow et al., 2010). Additionally supporting this argument, we find the topographically unconstrained and lithified sedimentary bed sites in Chautauqua (Site C) and northwestern Pennsylvania (Site B) have the least elongate bedforms, despite the potential for deformable substrates on these more easily erodible and mobile beds, indicating that distinct bedform morphologies are developed through topography. More specifically, it is the effect of topography on glacial conditions that allows for distinct bedform elongation to develop.

Topographically constrained regions also produce large variations in individual bedform surface relief (Figure 6), indicating less consistency in erosion and deposition distribution across the surface. This effect is particularly apparent at topographically constrained sites with easily eroded beds such as those in the Puget Lowland (Site A) and Bárðardalur (Site G; Figure 6). Large values of bedform surface relief in the Puget Lowland (Site A) may also be explained by the presence of isolated crystalline bedrock highs or the presence of bedforms on steep slopes (Spagnolo et al., 2012). However, due to the role of glacial ice in shaping these crystalline bedrock highs, and the significance of other metrics that correspond to large variations in bedform surface elevation, these features with large surface elevation changes were included in the final dataset. The streamlined bedforms present in the Bárðardalur valley (Site G) are lower in elevation than those found along the valley edges (Supporting Information Figure S1) and were therefore topographically controlled during ice thinning of the Icelandic Ice Sheet (Benediktsson et al., 2022). However, it is unlikely that the bedforms with the highest surface relief in Bárðardalur (Site G) are entirely composed of diamicton like the bedforms with smaller surface relief. We suggest the high relief bedforms in Bárðardalur (Site G) are comprised of diamicton overlying bedrock cores from pre-existing topography; however, further investigation of these features is needed to confirm this interpretation.

Topographically unconstrained sites with lithified sedimentary bed conditions create bedforms with the most uniform elongation and surface relief (Figure 6), indicating these regions are most suitable for

persistent, warm-based ice flow across the bed with well-developed processes of erosion and deposition in the subglacial environment (e.g., Benedikttson et al., 2016; Rattas & Piotrowski, 2003; Stokes et al., 2013). Lithified sedimentary sites that are topographically unconstrained have some of the greatest bedform densities (Table 2), highest orientation uniformity (Table 2; Figures 7 and 8), and smallest bedform relief and elongation, as previously mentioned (Figure 6), further suggesting these settings are favorable for persistent ice flow.

5 | CONCLUSIONS

The large, semi-automatically mapped dataset developed in this work provides key insight into topographic and bed lithology controls on ice flow properties that should be applied to understanding contemporary systems (King et al., 2009). The application of TPI developed in this study highlights its widespread ability to quickly map thousands of bedforms with little computational time, about half of the human error, and subjectivity with only a few shortcomings, including its difficulty in identifying low-relief, elongate subglacial bedforms across landscapes with prominent pre-glacial topography (Ebert et al., 2012; Hall et al., 2013). From the results of the dataset, we learn that landform signatures of warm-based ice flow have remarkable morphometric distribution similarities regardless of bed topography and lithology. All regions of ice flow, measurable by the presence of streamlined bedforms, are capable of similar ice-flow velocity distributions regardless of bed characteristics. However, we find that topographically constrained sites have the most elongate bedforms of the entire dataset, indicating that topography has a first-order control on ice flow velocity and persistence, controlling streamlined bedform elongation through topographic funneling (Eyles et al., 2018; Hall & Glasser, 2003; Hindmarsh, 2001; Ottesen et al., 2008; Roberts et al., 2010; Wellner et al., 2001). In this case, it is interpreted that substrate properties control the glaciological environment to develop bedforms with distinct high elongation.

While bedform elongation is controlled by topography, sites with sedimentary beds contain the greatest number and area of bedforms per area, indicating that bedrock lithology has a more dominant control on density and packing than bed topography. Topographically unconstrained sedimentary beds support formation and development of bedforms with uniform elongation ratios, low bedform surface relief, uniform bedform orientation and high bedform density, indicating that these sites are most suitable for the development of persistent ice flow with well-organized subglacial erosive and depositional processes.

Due to the fundamental role of bed topography and substrate in determining ice dynamics (Clarke et al., 1977; Cuffey & Paterson, 2010; Greenwood et al., 2021; Whillians & van der Veen, 1997), assessment of streamlined bedform morphologies provides crucial information on bed-related controls to ice flow (Stokes & Clark, 2001, 2002; King et al., 2009). As contemporary ice streams continue to retreat across environments with variable topography and bed lithology that are difficult to access and visualize, the use of preserved streamlined bedforms from paleo-subglacial environments is highly beneficial to constraining subglacial process sensitivities to variable bed conditions (Eyles et al., 2018; Greenwood et al., 2021; King et al., 2009; Stokes & Clark, 2001, 2002).

CONFLICT OF INTEREST

The authors have no conflict of interest to declare.

AUTHOR CONTRIBUTIONS

Project conceptualization, data curation, methodology, formal analysis, initial draft writing, writing-review, and editing were conducted by M. McKenzie. Conceptualization, funding acquisition, formal analysis, writing-review, editing, and supervision were conducted by L. Simkins. Partial conceptualization, writing-review, and editing were conducted by S. Principato. Partial data curation and editing were conducted by S. Munevar Garcia.

DATA AVAILABILITY STATEMENT

The datasets generated from this work are available on Pangaea Data Publisher for Earth and Environmental Science Repository (McKenzie et al., 2022: https://doi.org/10.1594/PANGAEA.939999). Published data include shapefiles of streamlined subglacial bedforms from the sites assessed in this work, an Excel file with all bedform morphometric raw data, and the ArcPython and toolbox file for the topographic position index (TPI) semi-automated landscape mapping tool.

All data generated stem from publicly available digital elevation models (DEMs) from Clallam County, 2005, for the Puget Lowland, Washington, USA site (https://lidarportal.dnr.wa.gov/#47.85003:-122.92053:7). The ArcticDEM data center was utilized for the M`Clintock Channel, Canada; Prince of Wales Island, Canada; Nunavut, Canada; Bárðardalur, Iceland; northern Norway; and northern Sweden sites (Porter et al., 2018: https://doi.org/10.7910/DVN/OHHUKH). United States Geological Society DEMs from 1999 and 2000 were used for the northwestern Pennsylvania, USA (http://www.pasda.psu.edu/), and Chautauqua, NY, USA sites (https://apps.nationalmap.gov/viewer/), respectively.

ORCID

Marion A. McKenzie 🅙 https://orcid.org/0000-0002-1130-4937

REFERENCES

Alden, W.C. (1905) The drumlins of southeastern Wisconsin. *United States Geological Survey Bulletin*, 273, 1–46. Available from: https://doi.org/10.3133/b273

Alley, R.B., Blankenship, D.D., Bentley, C.R. & Rooney, S.T. (1986) Deformation of till beneath ice stream B, West Antarctica. *Nature*, 322(6074), 57–59. Available from: https://doi.org/10.1038/322057a0

Bamber, J. & Aspinall, W. (2013) An expert judgement assessment of future sea level rise from the ice sheets. *Nature Climate Change*, 3(4), 424–427. Available from: https://doi.org/10.1038/nclimate1778

Benediktsson, Í., Aradóttir, N., Ingólfsson, Ó. & Brynjólfsson, S. (2022) Cross-cutting palaeo-ice streams in NE-Iceland reveal shifting Iceland Ice Sheet dynamics. *Geomorphology*, 396, 1–16. Available from: https://doi.org/10.1016/j.geomorph.2021.108009

Benediktsson, Í., Jónsson, S.A., Schomacker, A., Johnson, M.D., Ingólfsson, Ó., Zoet, L., Iverson, N.R. & Stötter, J. (2016) Progressive formation of modern drumlins at Múlajökull, Iceland: stratigraphical and morphological evidence. *Boreas*, 45(4), 567–583. Available from: https://doi.org/10.1111/bor.12195

Bourgeois, O., Dauteuil, O. & Vliet-Lanoë, B.V. (2000) Geothermal control on flow patterns in the Last Glacial Maximum ice sheet of Iceland. *Earth Surface Processes and Landforms: The Journal of the British Geomorphological Research Group*, 25(1), 59–76. Available from: https://doi.org/10.1002/(SICI)1096-9837(200001)25:1<59::AID-ESP48>3.0.CO;2-T

Briner, J.P. (2007) Supporting evidence from the New York drumlin field that elongate subglacial bedforms indicate fast ice flow. *Boreas*, 36(2), 143–147. Available from: https://doi.org/10.1111/j.1502-3885.2007.tb01188.x

Cazenave, P. W., Lambkin, D. O., & Dix, J. K. (2008). Quantitative bedform analysis using decimetre resolution swath bathymetry. In *CARIS 2008 International User Group Conference*.

Charlesworth, J.K. (1957) *The Quaternary Era: with special reference to its glaciation*. London: Arnold.

Clallam County, Olympic Department of Natural Resources, Washington Department of Transportation. (2008). *Puget Lowlands 2005* [data file]. Retrieved from https://lidarportal.dnr.wa.gov/#47.85003:-122.92053:7

Clark, C.D. (1993) Mega-scale glacial lineations and cross-cutting ice-flow landforms. *Earth Surface Processes and Landforms*, 18(1), 1–29. Available from: https://doi.org/10.1002/esp.3290180102

Clark, C.D. (1997) Reconstructing the evolutionary dynamics of former ice sheets using multi-temporal evidence, remote sensing and GIS. *Quaternary Science Reviews*, 16(9), 1067–1092. Available from: https://doi.org/10.1016/S0277-3791(97)00037-1

Clark, C.D. (1999) Glaciodynamic context of subglacial bedform generation and preservation. *Annals of Glaciology*, 28, 23–32. Available from: https://doi.org/10.3189/172756499781821832

Clark, C.D. (2010) Emergent drumlins and their clones: from till dilatancy to flow instabilities. *Journal of Glaciology*, 56(200), 1011–1025. Available from: https://doi.org/10.3189/002214311796406068

Clark, C.D., Ely, J.C., Spagnolo, M., Hahn, U., Hughes, A.L.C. & Stokes, C.R. (2018) Spatial organization of drumlins. *Earth Surface Processes and Landforms*, 43(2), 499–513. Available from: https://doi.org/10.1002/esp.4192

Clark, C.D., Evans, D.J.A. & Piotrowski, J.A. (2003) Palaeo-ice streams: an introduction. *Boreas*, 32(1), 1–3. Available from: https://doi.org/10.1080/03009480310001182

Clark, C.D., Hughes, A.L.C., Greenwood, S.L., Spagnolo, M. & Ng, F.S.L. (2009) Size and shape characteristics of drumlins, derived from a large sample, and associated scaling laws. *Quaternary Science Reviews*, 28(7–8), 677–692. Available from: https://doi.org/10.1016/j.quascirev.2008.08.035

Clarke, G.K.C., Nitsan, U. & Paterson, W.S.B. (1977) Strain heating and creep instability in glaciers and ice sheets. *Reviews of Geophysics*, 15(2), 129–255. Available from: https://doi.org/10.1029/RG015i002p00235

Cuffey, K. & Paterson, W.S.B. (2010) *The Physics of Glaciers*. Amsterdam, Netherlands: Elsevier.

De Rydt, J., Gudmundsson, G.H., Corr, H.F.J. & Christoffersen, P. (2013) Surface undulations of Antarctic ice streams tightly controlled by bedrock topography. *The Cryosphere*, 7(2), 407–417. Available from: https://doi.org/10.5194/tc-7-407-2013

Dowling, T.p.F., Spagnolo, M. & Möller, P. (2015) Morphometry and core type of streamlined bedforms in southern Sweden from high resolution LiDAR. *Geomorphology*, 236, 54–63. Available from: https://doi.org/10.1016/j.geomorph.2015.02.018

Ebert, K., Hall, A.M. & Hättestrand, C. (2012) Pre-glacial landforms on a glaciated shield: the inselberg plains of northern Sweden. *Norwegian Journal of Geology*, 92, 1–18.

Ely, J., Clark, C., Spagnolo, M., Stokes, C., Greenwood, S., Hughes, A., Dunlop, P. & Hess, D. (2016) Do subglacial bedforms comprise a size and shape continuum? *Geomorphology*, 257, 108–119. Available from: https://doi.org/10.1016/j.geomorph.2016.01.001

Evans, D., Phillips, E., Hiemstra, J. & Auton, C. (2006) Subglacial till: Formation, sedimentary characteristics and classification. *Earth-Science Reviews*, 78(1–2), 115–176. Available from: https://doi.org/10.1016/j.earscirev.2006.04.001

Eyles, N., Arbelaez Moreno, L. & Sookhan, S. (2018) Ice streams of the Late Wisconsin Cordilleran Ice Sheet in western North America. *Quaternary Science Reviews*, 179, 87–122. Available from: https://doi.org/10.1016/j.quascirev.2017.10.027

Eyles, N. & Doughty, M. (2016) Glacially-streamlined hard and soft beds of the paleo-Ontario ice stream in Southern Ontario and New York state. *Sedimentary Geology*, 338, 51–71. Available from: https://doi.org/10.1016/j.sedgeo.2016.01.019

Falcini, F.A.M., Rippin, D.M., Krabbendam, M. & Selby, K.A. (2018) Quantifying bed roughness beneath contemporary and palaeo-ice streams. *Journal of Glaciology*, 64(247), 822–834. Available from: https://doi.org/10.1017/jog.2018.71

Favier, L., Pattyn, F., Berger, S. & Drews, R. (2016) Dynamic influence of pinning points on marine ice-sheet stability: a numerical study in Dronning Maud Land. *East Antarctica. European Geosciences Union*, 10(6), 2623–2635. Available from: https://doi.org/10.5194/tc-10-2623-2016

Fowler, A.C. (2010) The formation of subglacial streams and mega-scale glacial lineations. *Proceedings of the Royal Society A: Mathematical, Physical and Engineering Sciences*, 466(2123), 3181–3201. Available from: https://doi.org/10.1098/rspa.2010.0009

Greenwood, S.L. & Clark, C.D. (2010) The sensitivity of subglacial bedform size and distribution to substrate lithological control. *Sedimentary Geology*, 232(3–4), 130–144. Available from: https://doi.org/10.1016/j.sedgeo.2010.01.009

Greenwood, S.L., Simkins, L.M., Winsborrow, M.C.M. & Bjarnadóttir, L.R. (2021) Exceptions to bed-controlled ice sheet flow and retreat from glaciated continental margins worldwide. *Science Advances*, 7(3), 1–12. Available from: https://doi.org/10.1126/sciadv.abb6291

Halberstadt, A., Simkins, L., Greenwood, S. & Anderson, J. (2016) Past ice-sheet behaviour: Retreat scenarios and changing controls in the Ross Sea. *Antarctica. Cryosphere*, 10(3), 1003–1020. Available from: https://doi.org/10.5194/tc-10-1003-2016

Hall, A.M., Ebert, K. & Hättestrand, C. (2013) Pre-glacial landform inheritance in a glaciated shield landscape. *Geografiska Annaler: Series A, Physical Geography*, 95(1), 33–49. Available from: https://doi.org/10.1111/j.1468-0459.2012.00477.x

Hall, A.M. & Glasser, N.F. (2003) Reconstructing the basal thermal regime of an ice stream in a landscape of selective linear erosion: Glen Avon, Cairngorm Mountains. *Scotland. Boreas*, 32(1), 191–207. Available from: https://doi.org/10.1111/j.1502-3885.2003.tb01437.x

Hättestrand, C., Gotz, S., Naslund, J.O., Fabel, D. & Stroeven, A.P. (2004) Drumlin formation time: evidence from northern and central Sweden. *Geografiska Annaler*, 86(2), 155–167. Available from: https://doi.org/10.1111/j.0435-3676.2004.00221.x

Hindmarsh, R.C.A. (2001) Influence of channelling on heating in ice-sheet flows. *Geophysical Research Letters*, 28(19), 3681–3684. Available from: https://doi.org/10.1029/2000GL012666

Hoffmann, H. (2015) violin.m - Simple violin plot using matlab default kernel density estimation. INRES (University of Bonn), Katzenburgweg 5, 53115 Germany. hhoffmann@uni-bonn.de

Hollingworth, S.E. (1931) The drumlins of Edenside and the Solway Basin. *Quarterly Journal of the Geological Society*, 87, 324–359.

Hughes, A., Clark, C. & Jordan, C. (2010) Subglacial bedforms of the last British Ice sheet. *Journal of Maps*, 6(1), 543–563. Available from: https://doi.org/10.4113/jom.2010.1111

Hughes, P., Gibbard, P. & Ehlers, J. (2013) Timing of glaciation during the last glacial cycle: Evaluating the concept of a global 'Last Glacial Maximum' (LGM). *Earth-Science Reviews*, 125, 171–198. Available from: https://doi.org/10.1016/j.earscirev.2013.07.003

Ignéczi, Á., Sole, A.J., Livingstone, S.J., Ng, F.S.L. & Yang, K. (2018) Greenland Ice Sheet Surface Topography and Drainage Structure

Controlled by the Transfer of Basal Variability. *Frontiers in Earth Science*, 6(101), 1–18. Available from: https://doi.org/10.3389/feart.2018.00101

King, E., Hindmarsh, R. & Stokes, C. (2009) Formation of mega-scale glacial lineations observed beneath a West Antarctic ice stream. *Nature Geoscience*, 2(8), 585–588. Available from: https://doi.org/10.1038/ngeo581

Kleman, J. & Borgström, I. (1996) Reconstruction of palaeo-ice sheets: The use of geomorphological data. *Earth Surface Processes and Landforms*, 21(10), 893–909. Available from: https://doi.org/10.1002/(SICI)1096-9837(199610)21:10<893::AID-ESP620>3.0.CO;2-U

Kleman, J., Hättestrand, C., Stroeven, A.P., Jansson, K.N., Angelis, H.D. & Borgström, I. (2006) Reconstruction of Palaeo-Ice Sheets- Inversion of their Glacial Geomorphological Record. In p.G. Knight (Ed.), *Glacier Science and Environmental Change*. Available from: https://doi.org/10.1002/9780470750636.ch38

Kleman, J. & Stroeven, A.P. (1997) Preglacial surface remnants and Quaternary glacial regimes in northwestern Sweden. *Geomorphology*, 19(1–2), 35–54. Available from: https://doi.org/10.1016/S0169-555X(96)00046-3

Krabbendam, M., Eyles, N., Putkinen, N., Bradwell, T. & Arbelaez-Moreno, L. (2016) Streamlined hard beds formed by palaeo-ice streams: A review. *Sedimentary Geology*, 338, 24–50. Available from: https://doi.org/10.1016/j.sedgeo.2015.12.007

Livingstone, S.J., Stokes, C.R., Cofaigh, C.Ó., Hillenbrand, C.-D., Vieli, A., Jamieson, S.S.R., Spagnolo, M. & Dowdeswell, J.A. (2016) Subglacial processes on an Antarctic ice stream bed. 1: Sediment transport and bedform genesis inferred from marine geophysical data. *Journal of Glaciology*, 62(232), 270–284. Available from: https://doi.org/10.1017/jog.2016.18

Maier, N., Humphrey, N., Harper, J., & Meierbachtol, T. (2019). *Sliding dominates slow-flowing margin regions*, Greenland Ice Sheet. Science Advances, 5, 5, 7, https://doi.org/10.1126/sciadv.aaw5406

Margold, M., Stokes, C.R. & Clark, C.D. (2015) Ice streams in the Laurentide Ice Sheet: Identification, characteristics and comparison to modern ice sheets. *Earth-Science Reviews*, 123, 117–146. Available from: https://doi.org/10.1016/j.earscirev.2015.01.011

Margold, M., Stokes, C.R. & Clark, C.D. (2018) Reconciling records of ice streaming and ice margin retreat to produce a palaeogeographic reconstruction of the deglaciation of the Laurentide Ice Sheet. *Quaternary Science Reviews*, 189, 1–30. Available from: https://doi.org/10.1016/j.quascirev.2018.03.013

McIntyre, N.F. (1985) The Dynamics of Ice-Sheet Outlets. *Journal of Glaciology*, 31(108), 99–107. Available from: https://doi.org/10.1017/S0022143000006328

McKenzie, M.A., Simkins, L.M. & Principato, S.M. (2022) Streamlined subglacial bedforms across the deglaciated Northern Hemisphere. *PANGAEA*. Available from: https://doi.org/10.1594/PANGAEA.939999

Menzies, J. (1979) A review of the literature on the formation and location of drumlins. *Earth Science Review*, 14(4), 315–359. Available from: https://doi.org/10.1016/0012-8252(79)90093-X

Ng, F.S.L. (1998). Mathematical Modelling of Subglacial Drainage and Erosion. *Unpublished thesis, St*. Catherine's College, Oxford.

Nienow, P., Sole, A., Slater, D. & Cowton, T. (2017) Recent Advances in Our Understanding of the Role of Meltwater in the Greenland Ice Sheet System. *Current Climate Change Reports*, 3(4), 330–344. Available from: https://doi.org/10.1007/s40641-017-0083-9

Ottesen, D., Stokes, C.R., Rise, L. & Olsen, L. (2008) Ice-sheet dynamics and ice streaming along the coastal parts of northern Norway. *Quaternary Science Reviews*, 27(9–10), 922–940. Available from: https://doi.org/10.1016/j.quascirev.2008.01.014

Payne, A. & Dongelmans, P. (1997) Self-organization in the thermomechanical flow of ice sheets. *Journal of Geophysical Research B: Solid Earth*, 102(6), 12219–12233. Available from: https://doi.org/10.1029/97JB00513

Pohjola, V.A. & Hedfors, J. (2003) Studying the effects of strain heating on glacial flow within outlet glaciers from the Heimefrontfjella Range, Dronning Maud Land, Antarctica. *Annals of Glaciology*, 37, 134–142. Available from: https://doi.org/10.3189/172756403781815843

Porter, C., Morin, P., Howat, I., Noh, M. J., Bates, B., Peterman, K., Keesey, S., Schlenk, M., Gardiner, J., Tomko, K., Willis, M., Kelleher, C., Cloutier, M., Husby, E., Foga, S., Nakamura, H., Platson, M., Wethington, M.. Williamson, C., Bauer, G., Enos, J., Arnold, G.,; Kramer, W., Becker, P., Doshi, A., D'Souza, C., Cummens, P., Laurier, F., & Bojesen, M., 2018, "ArcticDEM", https://doi.org/10.7910/DVN/OHHUKH, Harvard Dataverse, V1.

Principato, S., Moyer, A., Hampsch, A. & Ipsen, H. (2016) Using GIS and streamlined landforms to interpret palaeo-ice flow in northern Iceland. *Boreas*, 45(3), 470–482. Available from: https://doi.org/10.1111/bor.12164

Rattas, M. & Piotrowski, J.A. (2003) Influence of bedrock permeability and till grain size on the formation of the Saadjärve drumlin field, Estonia, under an east-Baltic Weichsealian ice stream. *Boreas*, 32(1), 167–177. Available from: https://doi.org/10.1080/03009480310001849

Rignot, E., Mouginot, J., Scheuchl, B., van den Broeke, M., van Wessem, M. J. & Morlighem, M. (2019) Four decades of Antarctic Ice Sheet mass balance from 1979-2017. *Proceedings of the National Academy of Sciences of the United States of America*, 116(4), 1095–1103. Available from: https://doi.org/10.1073/pnas.1812883116

Rippin, D.M., Vaughan, D.G. & Corr, H.F.J. (2011) The basal roughness of Pine Island Glacier, West Antarctica. *Journal of Glaciology*, 57(201), 67–77. Available from: https://doi.org/10.3189/002214311795306574

Roberts, D.H., Long, A.J., Davies, B.J., Simpson, M.J. & Schnabel, C. (2010) Ice stream influence on west Greenland ice sheet dynamics during the last glacial maximum. *Journal of Quaternary Science*, 25(6), 850–864. Available from: https://doi.org/10.1002/jqs.1354

Saha, K., Wells, N. & Munro-Stasiuk, M. (2011) An object-oriented approach to automated landform mapping: A case study of drumlins. *Computers and Geosciences*, 37(9), 1324–1336. Available from: https://doi.org/10.1016/j.cageo.2011.04.001

Schoof, C. & Clarke, G. (2008) A model for spiral flows in basal ice and the formation of subglacial flutes based on a Reiner-Rivlin rheology for glacial ice. *Journal of Geophysical Research: Solid Earth*, 113(5), 1–12. Available from: https://doi.org/10.1029/2007JB004957

Serrousi, H., Nakayama, Y., Larour, E., Menemenlis, D., Morlighem, M., Rignot, E. & Khazendar, A. (2017) Continued retreat of Thwaites Glacier, West Antarctica, controlled by bed topography and ocean circulation. *Geophysical Research Letters*, 44(12), 6191–6199. Available from: https://doi.org/10.1002/2017GL072910

Shaw, J., Kvill, D. & Rains, B. (1989) Drumlins and catastrophic subglacial floods. *Sedimentary Geology*, 62(2–4), 177–202. Available from: https://doi.org/10.1016/0037-0738(89)90114-0

Shaw, J., Pugin, A., & Young, R.R. (2008). A meltwater origin for Antarctic shelf bedforms with special attention to megalineations. *Geomorphology*, 102(3–4), 364–375, 364, https://doi.org/10.1016/j.geomorph.2008.04.005

Siegert, M.J., Taylor, J. & Payne, A.J. (2005) Spectral roughness of subglacial topography and implications for former ice-sheet dynamics in East Antarctica. *Global and Planetary Change*, 45(1–3), 249–263. Available from: https://doi.org/10.1016/j.gloplacha.2004.09.008

Spagnolo, M., Bartholomaus, T., Clark, C., Stokes, C., Atkinson, N., Dowdeswell, J., Ely, J., Graham, A., Hogan, K., King, E., Larter, R., Livingstone, S. & Pritchard, H. (2017) The periodic topography of ice stream beds: Insights from the Fourier spectra of mega-scale glacial lineations. *Journal of Geophysical Research: Earth Surface*, 122(7), 1355–1373. Available from: https://doi.org/10.1002/2016JF004154

Spagnolo, M., Clark, C.D., Ely, J.C., Stokes, C.R., Anderson, J.B., Andreassen, K., *et al.* (2014) Size, shape and spatial arrangement of mega-scale glacial lineations from a large and diverse dataset. *Earth Surface Processes and Landforms*, 39(11), 1432–1448. Available from: https://doi.org/10.1002/esp.3532

Spagnolo, M., Clark, C.D. & Hughes, A.L.C. (2012) Drumlin relief. *Geomorphology*, 153-154, 179–191. Available from: https://doi.org/10.1016/j.geomorph.2012.02.023

Spagnolo, M., Clark, C.D., Hughes, A.L.C. & Dunlop, P. (2011) The topography of drumlins; assessing their long profile shape. *Earth Surface Processes and Landforms*, 36(6), 790–804. Available from: https://doi.org/10.1002/esp.2107

Spagnolo, M., Clark, C.D., Hughes, A.L.C., Dunlop, P. & Stokes, C.R. (2010) The planar shape of drumlins. *Sedimentary Geology*, 232(3–4), 119–129. Available from: https://doi.org/10.1016/j.sedgeo.2010.01.008

Stokes, C.R. & Clark, C.D. (2001) Palaeo-ice streams. *Quaternary Science Reviews*, 20(13), 1437–1457. Available from: https://doi.org/10.1016/S0277-3791(01)00003-8

Stokes, C.R. & Clark, C.D. (2002) Are long subglacial bedforms indicative of fast ice flow? *Boreas*, 31(3), 239–249. Available from: https://doi.org/10.1080/030094802760260355

Stokes, C.R. & Clark, C.D. (2003) The Dubawnt Lake palaeo-ice stream: evidence for dynamic ice sheet behaviour on the Canadian Shield and insights regarding the controls on ice-stream location and vigour. *Boreas*, 32(1), 263–279. Available from: https://doi.org/10.1111/j.1502-3885.2003.tb01442.x

Stokes, C.R., Spagnolo, M., Clark, C.D., Cofaigh, C.Ó., Lian, O.B. & Dunstone, R.B. (2013) Formation of mega-scale glacial lineations on the Dubawnt Lake Ice Stream bed: 1. size, shape and spacing from a large remote sensing dataset. *Quaternary Science Reviews*, 77, 190–209. Available from: https://doi.org/10.1016/j.quascirev.2013.06.003

Tagil, S. & Jenness, J. (2008) GIS-Based Landform Classification and Topographic, Landcover and Geologic Attributes of Landforms Around the Yazoren Polje. *Turkey. Journal of Applied Sciences*, 8(6), 910–921. Available from: https://doi.org/10.3923/jas.2008.910.921

Tulaczyk, S., Lamb, W.B. & Engelhardt, H.F. (2000) Basal mechanics of Ice Stream B, West Antarctica 1. Till mechanics. *Journal of Geophysical Research*, 105(B1), 463–481. Available from: https://doi.org/10.1029/1999JB900329

United States Geological Survey (USGS). (1999). *7.5 minute Digital Elevation Model (10 meter resolution)* [data file]. Retrieved from https://apps.nationalmap.gov/viewer/

United States Geological Survey (USGS). (2000). *7.5 minute digital elevation models (DEM) for Pennsylvania 10 meter* [data file]. Retrieved from http://www.pasda.psu.edu/

Wang, S., Wu, Q. & Ward, D. (2017) Automated delineation and characterization of drumlins using a localized contour tree approach. *Int J Appl Earth Obs Geoinformation*, 62, 144–156. Available from: https://doi.org/10.1016/j.jag.2017.06.006

Weertman, J. (1957) On the sliding of glaciers. *Journal of Glaciology*, 3(21), 33–38. Available from: https://doi.org/10.1017/S0022143000024709

Weiss, A.D. (2001) Topographic Position and Landforms Analysis. In *Poster Presentation, ESRI User Conference, San Diego, CA* (Vol. 200), accessible online at http://www.jennessent.com/downloads/TPI-poster-TNC_18x22.pdf

Wellner, J.S., Lowe, A.L., Shipp, S.S. & Anderson, J.B. (2001) Distribution of glacial geomorphic features on the Antarctic continental shelf and correlation with substrate: implications for ice behavior. *Journal of Glaciology*, 47(158), 397–411. Available from: https://doi.org/10.3189/172756501781832043

Whillians, I.M. & van der Veen, C.J. (1997) The role of lateral drag in the dynamics of Ice Stream B, Antarctica. *Journal of Glaciology*, 43(144), 231–238. Available from: https://doi.org/10.1017/S0022143000003178

Winsborrow, M.C.M., Clark, C.D., & Stokes, C.R. (2010) What controls the location of ice streams? *Earth-Science Reviews*, 103(1–2), 45–59. Available from: https://doi.org/10.1016/j.earscirev.2010.07.003

Wright, W.B. (1912) The drumlin topography of South Donegal. *Geological Magazine*, 9(4), 153–159. Available from: https://doi.org/10.1017/S0016756800114141

Zoet, L.K., Rawling, J.E., III, Woodard, J.B., Barrette, N. & Mickelson, D.M. (2021) Factors that contribute to the elongation of drumlins beneath the Green Bay Lobe, Laurentide Ice Sheet. *Earth Surface Processes and Landforms*, 46(13), 2540–2550. Available from: https://doi.org/10.1002/esp.5192

SUPPORTING INFORMATION

Additional supporting information may be found in the online version of the article at the publisher's website.